Experimental Design of a Shock Tube
For the Time Response Study of Porous Pressure-Sensitive Paint

Thesis

Presented in Partial Fulfillment of the Requirements for Graduation with Distinction in the College of Engineering of the Ohio State University

By

David Huynh

Undergraduate Program in Aeronautical and Astronautical Engineering

The Ohio State University

2013

Honors Thesis Committee:

Professor James Gregory, Advisor

Professor Mei Zhuang

Abstract

This thesis summarizes the experimental design of a shock tube apparatus to study the time response of porous pressure sensitive paint (PSP). PSP is a relatively modern optical pressure measurement technique that is capable of providing nearly continuous surface pressure data. The recently developed porous PSP has exhibited very fast response times, on the order of microseconds, and is thus primed for application in unsteady flow studies. Much effort has been put into fully characterizing the dynamic response of porous PSP to most appropriately utilize it in future studies. This research was aimed to design and construct a shock tube for the purpose of later experimental evaluation of the time response of porous PSP and other PSP formulations. While the shock waves generated by shock tubes are commonly used to calibrate the response of fast instrumentation, this work looked to make use of the contact surface to study the PSP's response to pressure increases and pressure decreases. While there were many challenges in the design process and still many to overcome, the overall design of the shock tube was successful. Through continued development the device will be a fully capable tool for the study of the time response of PSP.

Acknowledgements

I am indebted to my research advisor, Professor James Gregory, who provided me with the opportunity, support, and guidance to conduct this research. I am incredibly grateful for the time and resources he has invested in my growth as a researcher and Aerospace Engineer. I would also like to thank Professor Mei Zhuang for her instruction in my undergraduate career. I have always appreciated her encouragement and I am very grateful to have her serving on my Honors Thesis Committee.

I could not have been as successful nor learned as much through the course of my research had it not been for the support of the graduate and undergraduate students in my research lab. I would like to thank graduate students Samik Bhattacharya, Kevin Disotell, Kyle Gompertz, Matt McCrink, and Di Peng as well as undergraduate students Matt Frankhouser, Kyle Hird, and Ryan McMullen for their roles in my undergraduate development.

I have been blessed with the unwavering support of my parents, Kim Pham and Hung Huynh, and girlfriend, Nikky Singhal, and I am truly grateful for their contributions to my progress.

Lastly, I would like to thank the College of Engineering for providing a scholarship in support of my research work.

Vita

January 18, 1991 .....Born, North Olmsted, Ohio, USA

May 5, 2013 .....B.S., Aeronautical and Astronautical Engineering, The Ohio State University

Field of Study

Major Field: Aeronautical and Astronautical Engineering

Table of Contents

List of Figures

List of Tables

Nomenclature

γ	ratio of specific heats (~1.4 for air, N_2, and O_2)
R	specific gas constant ($287.06\,\frac{J}{kgK}$ for air)
p_1	initial driven section pressure
T_1	initial driven section temperature
p_4	initial driver section pressure
T_4	initial driver section temperature
p_2	pressure after shock wave and before expansion fan
w	shock wave velocity
u_p	contact surface velocity
u_4	incident expansion fan velocity
u_5	reflected expansion fan velocity

Chapter 1: Introduction

In aerodynamic studies of complex flow, pressure distributions provide invaluable insight on unsteady phenomena. However, traditional pressure transducers provide only discrete pressure data, severely limiting the resolution of these distributions. In response to this limitation, an optical pressure measurement technique has recently been developed called pressure-sensitive paint (PSP). The paint responds to oxygen pressure and can provide continuous surface pressure data, a significant advantage over pressure transducers. Conventional PSP was limited by its slow time response, and further developments in PSP have led to a novel, porous binder that allows for very fast response times, on the order of microseconds. This porous PSP has many potential applications in unsteady aerodynamic studies. To best apply the technique, it is crucial to fully characterize how quickly and the manner in which the paint to responds to a change in pressure, referred to as its time response.

The long-term goals of this project are to study the time response of various formulations of porous PSP. The objective of this undergraduate research was to construct a shock tube apparatus to perform such studies in the future and gather preliminary data. Shock tubes create high-speed shock waves which are commonly used to calibrate fast-response instrumentation. However, this study aimed to utilize the contact surface generated by the shock tube to study the PSP's time response, an approach with many new benefits and challenges. One of the novel goals of this apparatus is to test the paint's response to a

rapid pressure decrease, which is typically very difficult to simulate and thus few studies have included this in their characterization. A great deal was learned during the design process of the shock tube and preliminary results indicate that there may be significant difference between the tested PSP's response to pressure increases and pressure decreases. The shock tube could provide a simple and effective method of studying PSPs in the future, which would bring the technique one step closer to becoming a ground-breaking tool in unsteady flow studies.

Chapter 2: Background

How PSP Works

PSP is an optical pressure measurement technique that consists of luminescent particles, called luminophores, embedded in an adhesive binder matrix. The luminophores can be brought from their ground state to a higher energy state by being exposed to an excitation light, typically via laser or LED (light-emitting diode). The particles then return to their ground state by one of two processes: luminescence, by which the luminophores release the energy as light, or oxygen quenching, whereby nearby oxygen molecules interact with and absorb the energy from the luminophores and prevent luminescence. The oxygen quenching phenomenon is what makes PSP a unique and powerful pressure measurement technique; at low pressures, fewer oxygen molecules are pressed the model surface, resulting in less oxygen quenching and thereby more luminescence, while at high pressures, more oxygen quenching and less luminescence occurs. This process is illustrated in Figure 1. Surface pressure can thus be inversely related to the paint's luminescent intensity. Because pressure measurements can be taken anywhere the PSP is applied, the paint offers a nonintrusive method to obtain highly spatially resolved surface pressure data as long as the model is optically accessible.

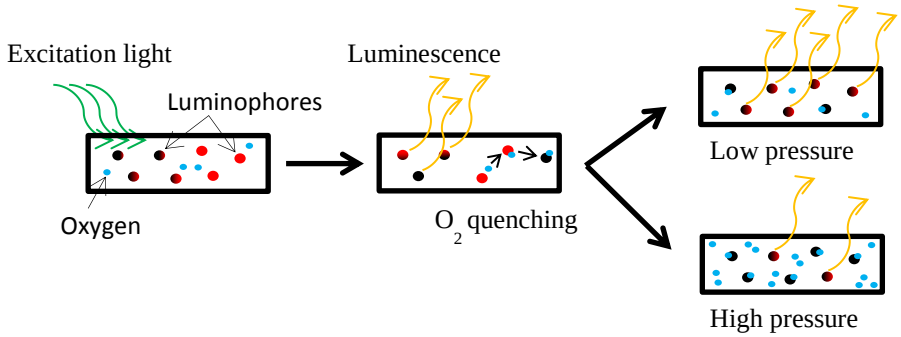

Figure 1: Illustration of how PSP operates

Conventional PSP vs. Porous PSP

Conventional PSPs use a polymer as the binder matrix material. In these paints, oxygen molecules must diffuse through the polymer binder before being able to interact with the luminophores, restricting the paints' response time. Conventional PSPs have been observed to have response times on the order of seconds, which, while suitable for steady flow studies, is not suitable for unsteady aerodynamic studies. In response to this limitation, significant efforts were made to create new binders to allow for faster response times. As a result, a binder was developed in which the luminophores sit on the surface of pores in the material, as illustrated in Figure 2. This porous PSP allows the luminophores to interact directly with local oxygen molecules, resulting in response times on the order of microseconds (Sakaue 2001). However, as previously mentioned, it is critical to fully understand the time response characteristics of porous PSP in order to best apply it. While previous studies have evaluated the response of porous PSP to rapid increases in pressure, simulating a rapid decrease in pressure is challenging. Thus, paint's response to a rapid decrease in pressure still remains to be characterized.

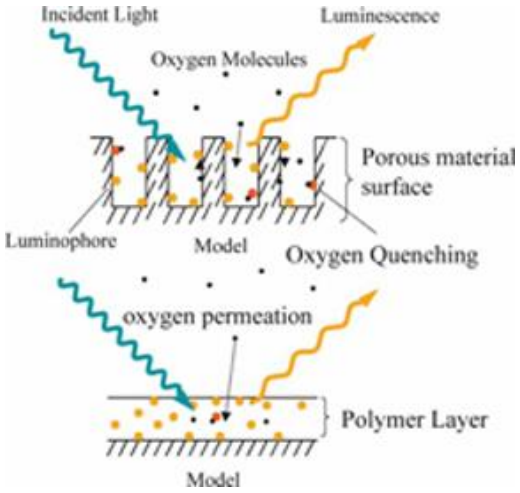

Figure 2: Illustration of porous PSP (top) vs. conventional PSP (bottom)

How Shock Tubes Work

Shock tubes are popular devices to evaluate the dynamic response of instrumentation. A shock tube is a long tube, made up of a high-pressure driver section and low-pressure driven section separated by a diaphragm, illustrated in Figure 3.

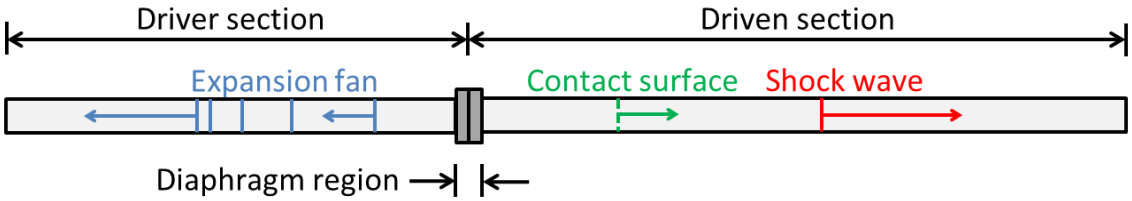

Figure 3: Illustration of a shock tube

Traditionally the driver section is referred to as upstream of the diaphragm and the driven section downstream. When the diaphragm material is broken, either by pressure difference or alternate mechanism, the resulting instantaneous pressure ratio generates a downstream-traveling shock wave and an upstream-traveling expansion fan. The interface between the driver and driven gases induced by the shock wave, called the

contact surface, also propagates downstream following the shock. All of the phenomena travel very quickly, with the shock wave and expansion wave traveling faster than the speed of sound and the contact surface capable of Mach 0.3-0.5, depending on the initial pressure ratio (Anderson 2004).

The shock wave provides a nearly instantaneous step change increase in pressure, temperature, and density. Properties change continuously over the expansion fan. The contact surface has a step change in temperature and density across it; however, pressure and velocity are preserved. The changes in air properties over the shock tube phenomena are illustrated in Figure 4. The speeds and strengths of these shock tube phenomena are functions of the initial pressure ratio across the diaphragm, defined as driver pressure (p_4) divided by driven pressure (p_1). Note this is pressure ratio (p_4/p_1), not pressure difference ($p_4 - p_1$).

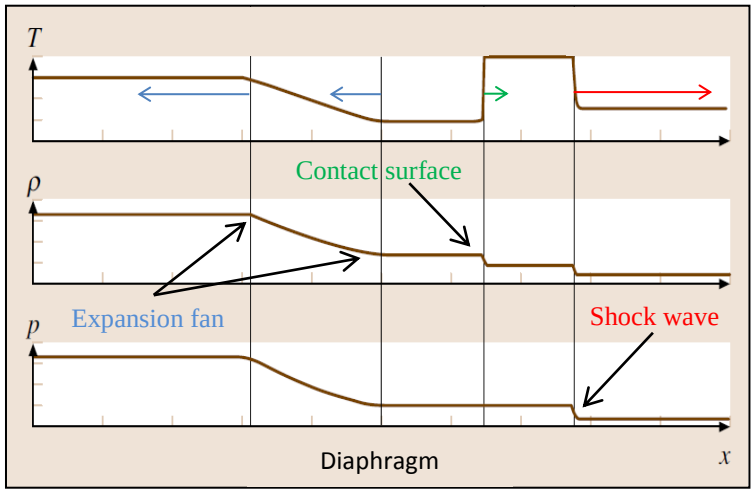

Figure 4: Illustration of the changes in static air properties
(top to bottom: temperature, T; density, ρ; pressure, p) across the shock tube phenomena

Chapter 3: Experimental Design

Motivation and Design Challenges for Shock Tube

Recall that PSP operates based on local oxygen pressure. This means a change in pressure for the PSP can be generated by an actual change in pressure or by a change in oxygen concentration. Exploring the latter observation, this indicates that a pressure decrease can be simulated by reducing oxygen concentration. Enter the shock tube and the generated contact surface. The contact surface is a high-speed interface between the driver and driven gas. If the driver and driven gas were at different oxygen concentrations, the contact surface would simulate a rapid pressure change as it passed across the PSP. This would allow for a study of the time response of a PSP sample for both rapid pressure rises and falls by having the driver and driven sections with different gas compositions/oxygen concentrations.

While in principle this concept is very simple, there several factors that complicate the design of this shock tube apparatus. Many difficulties stem from the contact surface, which is heavily affected by viscosity and boundary layer effects (Mirels 1963) as well as diaphragm bursting characteristics (Rothkopf 1974). These effects result in the contact surface being distorted and non-uniform, making the change in test gas composition less rapid and less consistent. The diaphragm and bursting mechanism are significant challenges as most previous work with shock tubes has been conducted with high pressure ratios and thus much stronger and robust diaphragms. A design choice of this

research was to operate at low pressure ratios, for safety, convenience, and cost considerations. Thus, the diaphragm material and bursting mechanism for this project had to be studied without much of a base from previous work.

Initial Shock Tube Requirements and Design Decisions

The initial concept of the experimental set-up was an inexpensive, "table-top" shock tube, around or less than 2 meters (~6.5 feet) in length. This size of shock tube was on the scale of the apparatus used by Sakaue et. al (Sakaue 2001), and so Sakaue's device was used as a baseline design. Sakaue's shock tube was about 1 meter (~3.3 feet) and operated with the driver section at ambient pressure (~14.7 psi) and the driven section vacuumed to a desired low pressure (~3.71 psi). Sakaue ran at a pressure ratio of 4 and broke an aluminum diaphragm via pressure difference.

The initial length of this study's shock tube was selected to be 5 feet. It was found that PVC piping was an inexpensive and suitable material for the experiment's needs, able to support 200 psi (Home Depot n.d.), significantly greater than the expected experimental pressures. Using PVC piping restricted the cross section of the tube to be circular. A key design choice was making the shock tube open-ended at the end driven end. This decision was motivated by the thought that the generated shock wave would exit the shock tube and not be reflected, allowing more test time for the contact surface. The initial driven section pressure was thus constrained to be ambient pressure. Also, with the driven section open, the driver section would have to be pressurized to create the desired pressure ratio. With the shock wave exiting the shock tube, it was decided to keep the pressure ratio fairly low, around 2, to reduce the shock strength of safety

concerns. A lower pressure ratio also allowed the shock tube to consume less pressurized gas, reducing costs.

Preliminary Analytical Study

With the total length of the shock tube and pressure ratio selected, the appropriate lengths of the driver and driven sections was calculated using the 1-D, inviscid theory presented by Anderson (Anderson 2004). See Appendix A for a brief description of the theory. This theory was used to determine the shock wave, contact surface, and expansion fan velocities given an initial pressure ratio. These velocities were then applied to the shock tube. The limiting factors on the test time of the shock tube were the time between passages of the shock wave and the contact surface through the test section and the time between the passages of the contact surface and the expansion fan through the test section, which for convenience will be referred to as t_1 and t_2, respectively. t_1 needed to be large enough to allow the PSP to fully respond to the step change across the shock wave and t_2 need to be large enough to record the PSP's response to the contact surface before the expansion fan passed and introduced a gradual pressure decrease.

It was decided that t_1 and t_2 would be made equal to temporally isolate the contact surface from the other pressure phenomena. A MATLAB script was written to iterate through various driver/driven length ratios and calculate the corresponding shock tube velocities and test time to yield the maximum test time. See Appendix B for the MATLAB code. The optimal driver/driven ratio was determined to be roughly 0.75/0.25, or 3.75 feet/1.25 feet for a 5 foot tube for a pressure ratio of 2. The corresponding x-t diagram, illustrating the spatial propagation of the shock tube phenomena through time, is shown in Figure 5.

Note that this study assumed that the shock wave would exit the tube and not reflect back into the driven section.

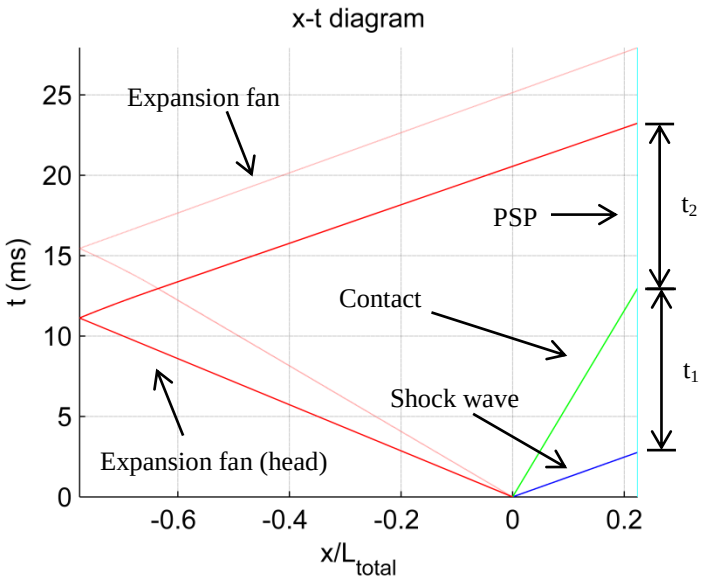

Figure 5: x-t diagram for L_{driver}/L_{driven} yielding maximum test time

First Phase Design: Shock Tube Construction

Using the parameters determined in the preliminary analysis, the first shock tube design was constructed of 2" inner diameter PVC tubing, with driver and driven lengths 3.75 feet and 1.25 feet, respectively. A Kulite pressure transducer was placed perpendicular to the flow at the end of the driven section, where the test section would be placed. The Kulite data was recorded using a Waverunner oscilloscope. A thin sheet of acetate was used as the diaphragm material and a pointed, metal rod was used as the bursting mechanism. A more detailed study of the diaphragm material and bursting mechanism was performed later and is described in the following section. A rapid spike in pressure

was observed, shown in Figure 6, which was contrary to the expected step change in pressure as described in the Background section. This was reasoned to be the result of ambient air rushing in to return the driven section to ambient pressure after the shock exited.

In response, an additional 5 feet was added downstream of the test section to prolong this pressure equalization passed the time window of interest. Looking at Figure 7, it is clear that the additional tubing allowed the increase in pressure to be sustained. Here, the shock wave and the expansion fan are clearly resolved; recall that pressure does not change across the contact surface and thus the contact surface is not represented in the Kulite data. The slight bump in the expansion fan around 9 ms was the result of a second expansion fan propagating back upstream into the shock tube. This second expansion fan was generated as the initial shock wave exited the driven section; as the shock wave left the tube, the pressurized air just upstream of the shock interacted with the ambient air, analogous to a second diaphragm burst. This second interaction formed a second expansion fan traveling back into the shock tube, which collided with and added to the first expansion. This explanation was arrived at through experimental results as well as computational results from a second-order upwind scheme (Huynh 2003) and was eventually supported by literature from previous shock tube studies (Gordon/Hall 1959).

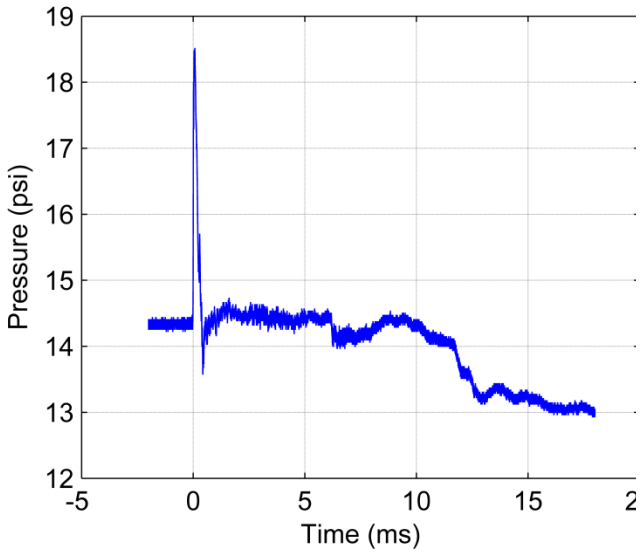

Figure 6: Kulite data at the end of driven section for first iteration shock tube

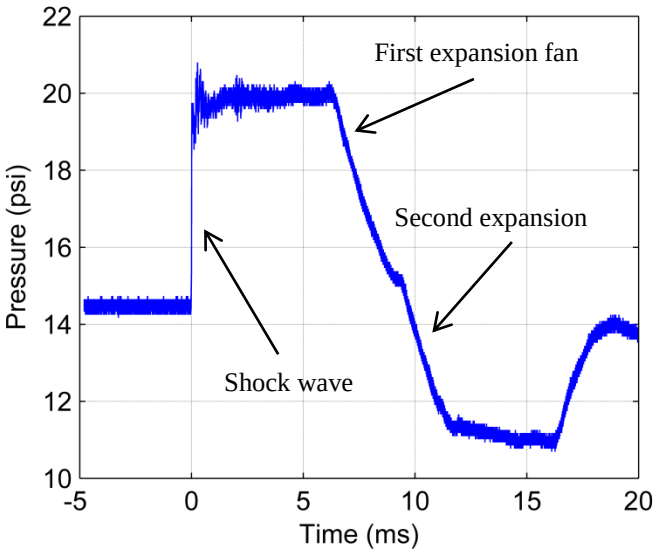

Figure 7: Kulite data at test section for lengthened driven section

Diaphragm Study: Material and Bursting Method

Potentially the most critical aspect of the shock tube design was the diaphragm material and bursting method. This is because previous shock tube studies have shown that the planarity and quality of the contact surface are heavily dependent on the diaphragm characteristics. In basic shock tube theory, when the diaphragm is burst, it instantaneously and uniformly disappears. In reality, the most ideal diaphragm bursts into the four-pedal formation, where the four equal pedals simultaneously fold out flush to the tube walls. This type of burst has been observed to generate the most uniform shock waves and contact surfaces (Rothkopf 1974). In addition to the uniform phenomena, the four-pedal burst also retains the diaphragm, with no shrapnel traveling downstream. This aspect was important because the PSP study requires constant optical access. If the four-pedal formation was not achievable, it was determined that upon

bursting, as much area from the diaphragm should break as quickly as possible, with minimal material traveling down the shock tube.

Three diaphragm materials were considered: metallic dura-lar film (the material of metallic balloons), acetate (thin, transparent plastic; similar to overhead projector slides), and aluminum foil. Likewise, three bursting methods were evaluated: bursting via physical plunger, heating, and pressure difference. The plunger used was a pointed, metal rod. The heating method entailed a thin nichrome wire making contact with the diaphragm, through which a current was applied, heating the nichrome wire and weakening the diaphragm to the point that the pressure broke the material.

The dura-lar film was ruled out because the material was too strong and did not burst even after being punctured with the plunger. The aluminum foil proved to be too weak as it tended to break into many pieces and travel downstream. Though the plunger was a very simple and consistent mechanism to break the diaphragm, it was a significant body in the flow and could also limit optical access to the test section and so was not selected. Bursting via pressure difference was found to be inconsistent and, with the exception of aluminum foil, required a large driver pressure to break the diaphragm. Thus, the diaphragm material was chosen to be acetate and the bursting mechanism heating through a nichrome wire.

The nichrome wire was stretched across the downstream end of the acetate sheet. This way, when the acetate bulged from the driver section pressure, it would be pressed into contact with the wire. Upon bursting, the acetate did not fold into the four-pedal formation; like the aluminum, the acetate tended to tear. However, the acetate was stronger than the aluminum and tore into fewer, larger pieces. By simply applying an

adhesive to the acetate, when the diaphragm burst, the material would tear, flap open, and the torn shrapnel would be retained by the tape. Multiple nichrome wire orientations were explored: the nichrome was stretch across a diagonal, across a secant, around the circumference, and in a cross. The secant-orientation, illustrated in Figure 8, was found to be the best positioning as it consistently removed the greatest amount of material upon bursting.

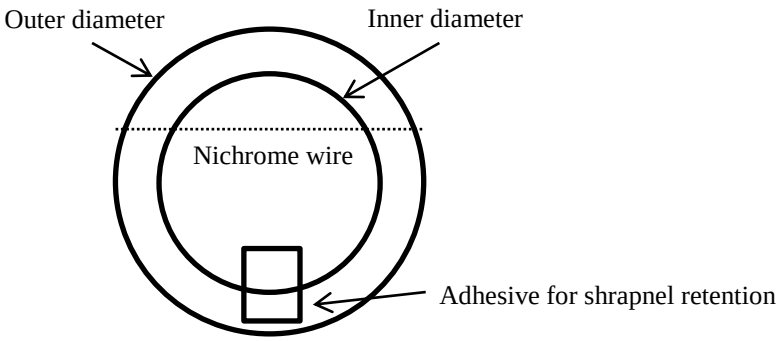

Figure 8: Illustration of nichrome wire across diaphragm

Second Phase Design: Contact Surface Detection

After determining the diaphragm apparatus and acquiring consistent pressure data, the test section for the PSP was added to the shock tube. A 2” inner diameter cast acrylic tube was selected for the test section for its transparency and machinability. The acrylic was cut to a 1.5” length; the short length was necessary in order to paint the inside of the section. However, before the PSP was integrated into the experiment, an extensive study was performed on the contact detection.

Detection of the contact surface was by far the most challenging aspect of the design. Because static pressure and velocity are constant across the contact, only instrumentation sensitive to total pressure, temperature, or density were applicable. All temperature sensors that were considered were found to be too slow (thermocouples), too fragile (hot wires), or too expensive (infrared temperature sensors). A total pressure pitot probe was tested and displayed a fast enough response to capture the shock wave; however, the change in total pressure was too small to be observed, as seen in Figure 9.

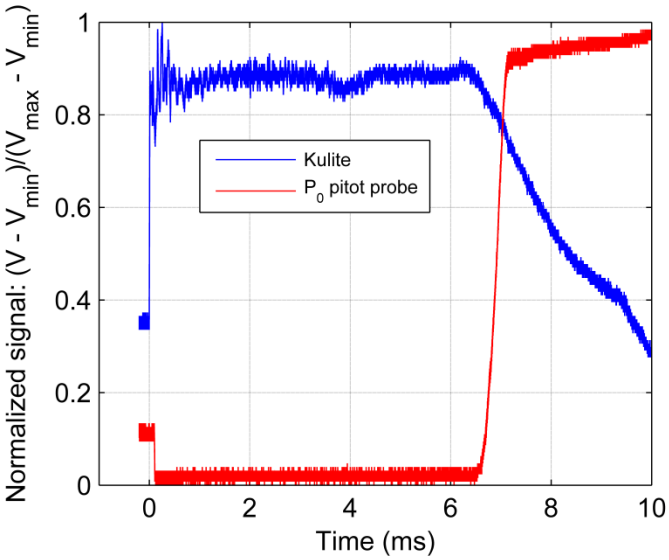

Figure 9: Kulite (blue) and total pressure pitot probe (red)

As the density changes, so does the index of refraction; in fact, index of refraction is related to the spatial gradient of density (Settles 2006). Thus, a small change in density over a very small distance, such as across a shock or contact surface, there will be large change in index of refraction. Using this idea, a 532 nm (green) laser diode was positioned to fire a laser through the test section onto a photodetector. The photodetector output a voltage corresponding to the spatial position of the laser, with left being more

negative and right being more positive. Thus, as the shock wave or contact surface passed the test section, the increase in density and index of refraction would refract the laser upstream, which would be registered by the photodetector as a brief and rapid decrease in voltage (assuming left upstream). Though it would be very difficult to extract the magnitude of the density gradient across the shock or contact using this method, only the time data was necessary. The photodetector laser diode was positioned such that the laser passed through the cross-sectional plane of the Kulite to ensure the signals would be temporally synchronized.

A representative plot of the photodetector data is displayed in Figure 10, with the photodetector data in blue and the contact surface prediction from the 1-D theory in red. The shock wave was well resolved as seen by the sharp spike downward, which corresponded well to the pressure increase in the Kulite signal in Figure 11. There appeared to be some slight oscillations in the photodetector near the predicted contact time, though closer inspection in Figure 12 revealed a noisy signal with no obvious representation of when contact begins passing through the test section. Moreover, looking at Figure 13, multiple runs displayed a few common characteristics, such has the spike corresponding to the shock wave and an increase in oscillations near the predicted contact surface time, but also very distinct long-time scale patterns. This made the characterization of the contact surface little more than speculation, as the signal noise could vary from run to run as well as be a result of a non-uniform contact surface.

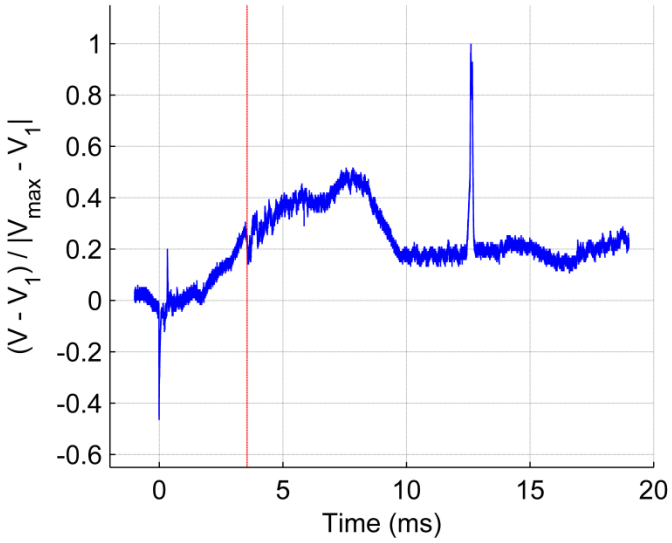

Figure 10: Photodetector data (blue) with predicted contact time (red)

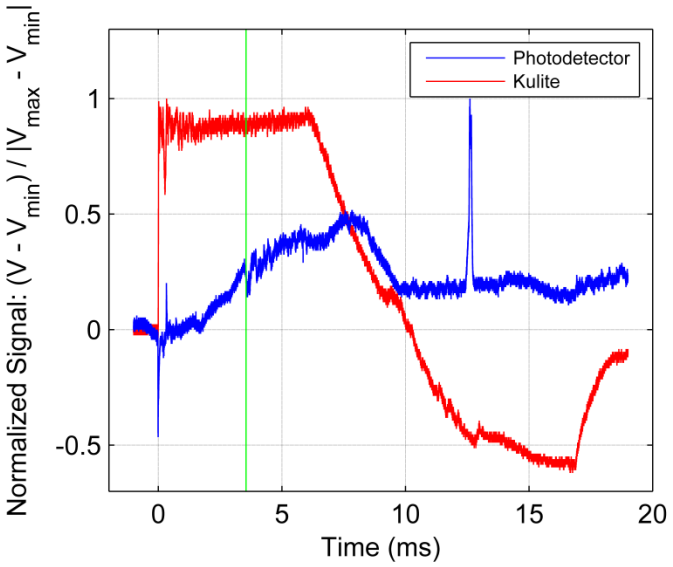

Figure 11: Photodetector (blue), Kulite (red), and predicted contact time (green)

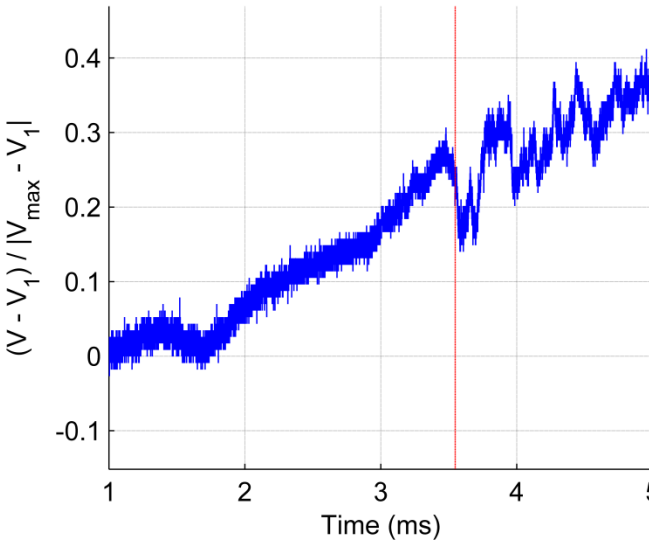

Figure 12: Photodetector (blue) and predicted contact time (red), zoomed in to contact surface prediction

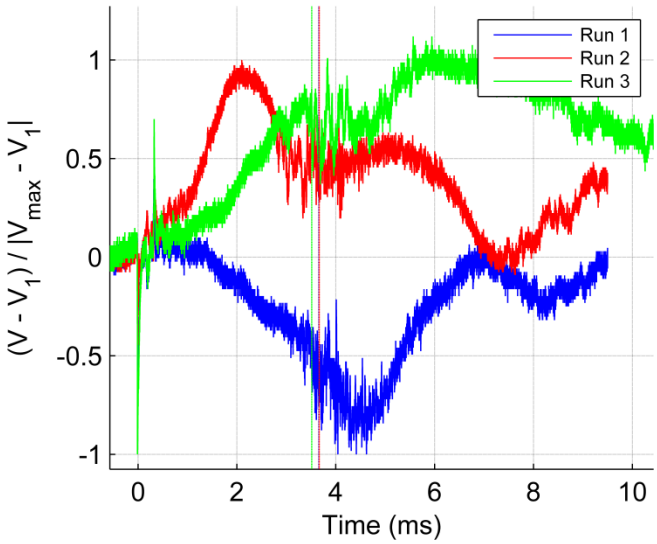

Figure 13: Photodetector data, multiple runs

Despite the inconclusive contact detection study, it was decided to proceed to the PSP phase of the design as it was possible that the PSP's response could help illuminate the contact surface.

Chapter 4: Current Experimental Set-up and Preliminary PSP Results

Integration of PSP into Experimental Set-up

One fourth of the test section's circumference was coated in PtTFPP, the paint formulation used by Dr. James Gregory's research group at the Aeronautical and Astronautical Research Labs (see Figure 14 for a photograph). A high-powered 532 nm laser was selected as the excitation source and a photomultiplier tube (PMT) was selected as the instrument to record the luminescence. The PSP, laser, and PMT were integrated into the current experimental set-up, illustrated in Figure 15. See Appendix C for photographs of the experimental set-up.

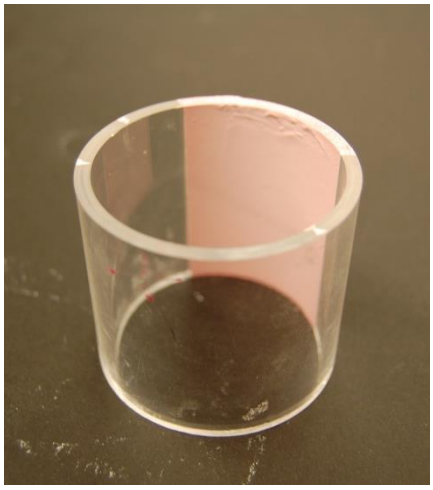

Figure 14: Photograph of test section painted with PSP

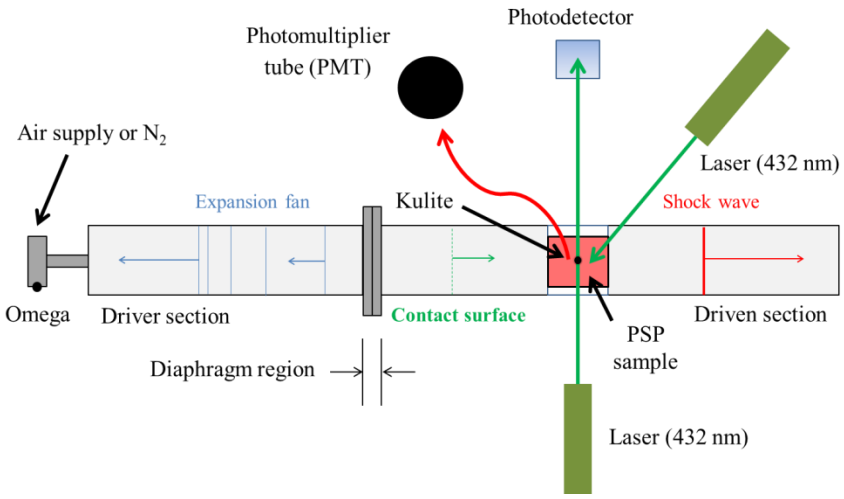

Figure 15: Current experimental set-up

With the PSP in the test section, the driver section was pressurized with nitrogen gas to simulate the pressure decrease across the contact surface. The excitation laser was positioned such that the excitation spot was in the same plane with the Kulite and photodetector laser so all three signals would line up temporally. Because the PMT was so sensitive to light and could be easily damaged, all data with the PSP was taken with all doors closed and all lights off except the lasers. Once the optics were set up, the driver pressure was recorded by the Omega pressure transducer for the analytical contact prediction. The circuit with the nichrome wire was then closed, heating the wire and bursting the diaphragm. An oscilloscope recorded the data from the Kulite, photodetector, and PMT; the system was triggered by the shock wave in the Kulite signal. To most meaningfully compare the PSP's time response to a pressure increase to its time response to a pressure decrease, it was important to keep the magnitude and quality of the pressure change the same and simply switch the direction. This study utilized the contact surface as a pressure decrease; the driver section was filled with a pressurized

nitrogen/air mixture and the driven section was left open to atmospheric air. For clarity, this will be referred to as configuration 1, where downstream of the contact is air and upstream is a nitrogen/air mixture. In consideration of future studies, a process to reverse the gas composition across the contact surface was devised, which will be referred to as configuration 2. In configuration 2, the driver section would be pressurized using shop air to match the driver pressure in configuration 1 (to generate phenomena of equal speed and strength) and also match the driven oxygen concentration in configuration 1, which was also air. The driven section in configuration 2 would then be brought to the same nitrogen/air concentration of the driver section in configuration 1 through a process called purging. A nitrogen supply and an air supply would each be regulated to the appropriate pressures to create the desired nitrogen/air ratio. The two supplies would be hosed together and the gasses allowed to mix. This mixture would then flood the driven section, downstream of the diaphragm and upstream of the test section. A finite amount of time would be given for the purging process to fully saturate the driven section with the mixture. Once saturation was reached, the purging would be stopped and immediately after the shock tube fired, so as to not allow time for the ambient air to propagate up the driven section. This would create a contact surface with a downstream nitrogen/air mixture and upstream air while maintaining the same pressure ratio as configuration 1, simulating the equivalent pressure increase case to configuration 1's pressure decrease. Table 1 summarizes the conceptual set-up for each configuration.

Table 1: Summary of experimental configurations to control change gas composition across contact surface

	Driver pressure	**Driver gas**	**Driven pressure**	**Driven gas**	**ΔO_2% across contact**
Configuration 1	32 psi	N_2/air	14.7 psi	Air	Decrease
Configuration 2	32 psi	Air	14.7 psi	N_2/air	Increase

Preliminary Results for PSP Time Response Study

The PSP resolved the shock wave very clearly as a step decrease in voltage as seen in Figure 16, with the PSP data in blue and the predicted contact time in red. Examining the shock save more closely in Figure 17, it was seen that the PSP's response was an exponential decay, with a rapid drop in voltage immediately after the shock and then decaying to a final steady-state value. The paint appeared to have a response time around 0.1 ms or 100 μs. Near the predicted contact time, the PSP appeared to have a significant increase in voltage, which would correspond to the drop in oxygen concentration across the contact. The PSP appeared to have an exponential decay response to the contact, similar to the shock, though on a much longer time scale, on the order of 1-2 ms. However, precise information on the paint's time response was not clear because the paint did not decay into a steady-state level, but rather continued increasing in voltage. Plotting the PSP data with the Kulite data in Figure 18 it was observed that the PSP responded to the expansion fan and that the expansion fan may have passed the PSP before it was able to fully respond to the contact surface. This made it very challenging to confidently extract time response information.

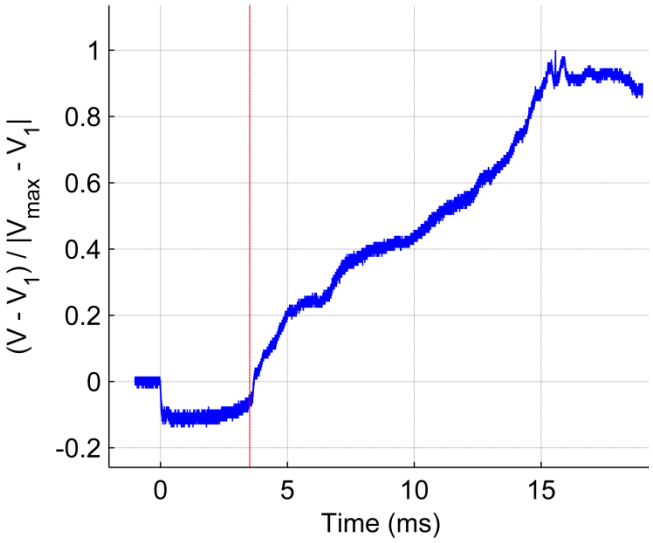

Figure 16: PSP (blue) and predicted contact time (red)

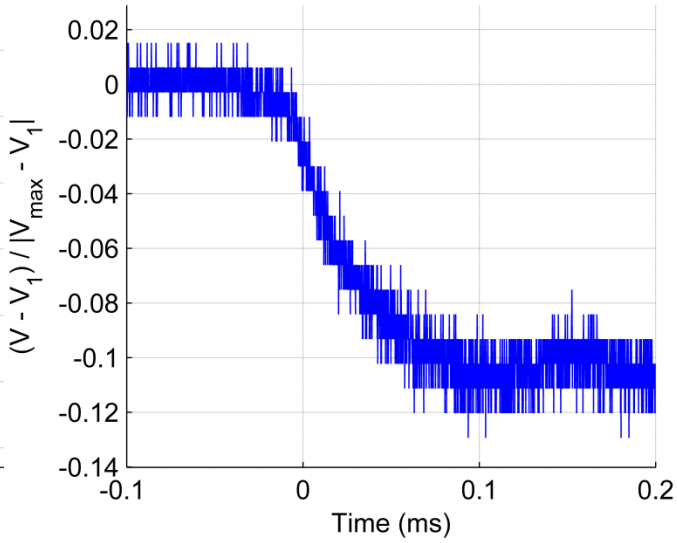

Figure 17: PSP data, zoomed to shock wave

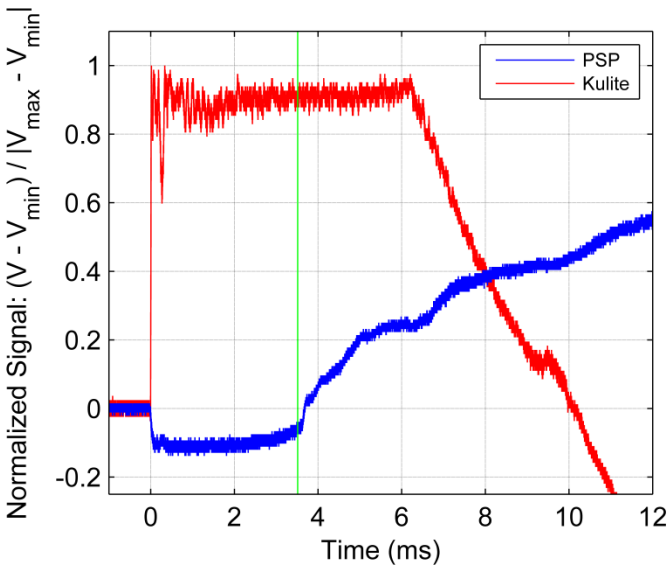

Figure 18: PSP (blue), Kulite (red), predicted contact time (green)

Juxtaposing the PSP data with the photodetector data revealed that, if the oscillations in the photodetector did indicate the contact surface, the PSP had a significant time delay associated with it. Figure 19 shows the PSP and photodetector data together and Figure 20 shows the oscillations in the photodetector preceded the jump in the PSP by between

0.25 ms to a full millisecond, depending on which spike was taken to represent the beginning of the contact surface. Interestingly, if this truly was a time delay in the PSP's response, it occurred with only with the pressure decrease of the contact surface; the paint's response to the shock wave matched up very closely to the Kulite's signal, showing no time delay.

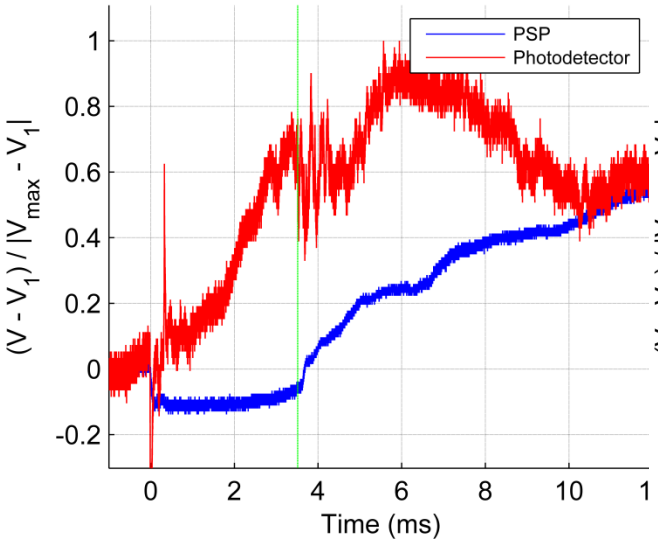

Figure 19: PSP (blue), photodetector (red), and predicted contact time (green)

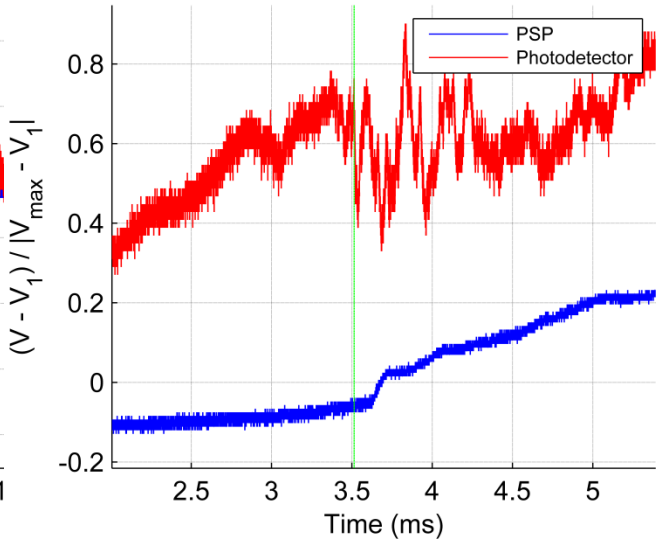

Figure 20: PSP and photodetector, zoomed near predicted contact time

Chapter 5: Discussion and Conclusions

Designing and constructing the shock tube for future PSP study proved to be a very challenging and instructive process. The initial design decision to have the driven end be open to avoid the reflected shock wave was found to be slightly misguided; though the open end did prevent the shock wave reflection, as the shock exited the tube, it acted like a second diaphragm burst and sent a second expansion fan traveling back upstream. In retrospect, a semi-infinite shock tube rather than an open shock tube would have avoided both the reflected shock wave and second expansion fan, though this has obvious implementation issues. The second expansion fan did not interfere with the PSP study, though it was an interesting discovery in the shock tube development.

As predicted, the contact surface presented several challenges to the experimental method. After eliminating several detection instruments, it was decided that a photodetector would be used to detect the refraction of a laser through the test section caused by the change in density over the contact surface. However, it was observed that the contact was very difficult to identify in the photodetector data due to the noisy signal. Though there did appear to be some notable patterns in the signal that were suspected to be the contact surface, it was unclear when the contact surface began. This obscurity could have been the result of a non-uniform contact surface or a limitation in the detection method itself.

Despite the struggles in contact detection, the preliminary results from the porous PSP were very promising. The PSP was able to resolve the shock wave and was in close agreement with the Kulite data. Based on the response to the shock, the PSP appeared to have a response time on the order of 100 μs, a result in close agreement with results of previous studies (Gregory et al. 2008 & Sakaue 2001). The PSP also responded to the contact surface, though much more slowly. It was unclear whether the slow response was due to the PSP's limitations or the result of a non-uniform contact surface, making the analysis of the time response inconclusive. In future studies, it would be beneficial to operate the shock tube such that there is more time between the contact surface and the expansion fan to give the PSP more time to respond to the contact surface. This can be achieved by increasing the pressure ratio across the diaphragm or moving the test section more upstream.

The shock tube design was successful in a number of ways. The diaphragm and bursting method provided consistent and controlled operation of the shock tube. The pressure phenomena were clearly resolved by the Kulite pressure transducer and the shock wave provided a reliable means of triggering the data acquisition. The test sections were designed in such a way that they were easily removed from the tube and reused for different PSP formulations. The shock tube was secured to the table, minimizing recoil from the diaphragm burst. The PSP data indicated a need to further develop the apparatus to isolate the contact surface, but was encouraging nonetheless. I am confident that I will be able to bring the shock tube to full functionality before my graduation this year.

Outside of its application in studies of PSP, the shock tube would be very useful and instructive as an undergraduate academic lab. Without the optical set-up, the shock tube was inexpensive, simple to construct, and very illustrative of fundamental compressible flow. It is my hope that my research can provide future students an opportunity to see their studies applied.

Chapter 6: References

Anderson, J.D. "Modern Compressible Flow With Historical Perspective." 261-302. McCraw-Hill, 2004.

Gordon/Hall, I. I. Glass and J. "Section 18: Shock Tubes." In *Handbook of Supersonic Aerodynamics*. Bureau of Naval Weapons, 1959.

Gregory, J W, K Asai, M Kameda, T Liu, and J P Sullivan. "A review of pressure-sensitive paint for high-speed and unsteady aerodynamics." *Journal of Aerospace Engineering*, 2008: 249-290.

Home Depot. n.d. http://www.homedepot.com/p/t/100161954?catalogId=10053&langId=-1&keyword=pvc+pipe+2%22&storeId=10051&N=5yc1v&R=100161954#specifications (accessed June 27, 2012).

Huynh, H.T. "Analysis and improvement of upwind and centered schemes on quadrilateral and triangular meshes." *AIAA Paper 2003-3541*, 2003.

Mirels, Harold. "Test Time in Low Pressure Shock Tubes." *Physics of Fluids*, 1963: 1201-1214.

Rothkopf, E.M. and Low, W. "Diaphragm opening process in shock tubes." *Physics of Fluids*, 1974: 1169-1173.

Sakaue, H. and Sullivan, J.P. "Time Response of Anodized Aluminum Pressure-Sensitive Paint." *AIAA 39(10)*, 2001: 1944-1949.

Settles, G.S. *Schlieren & Shadowgraph Techniques.* Springer, 2006.

Appendix A: Shock Tube Theory

Traditionally, shock tube theory follows the following notation:

Before diaphragm bursts:

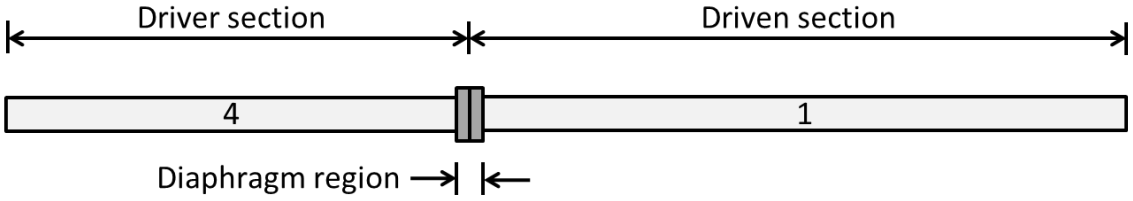

After burst, before expansion fan reflection:

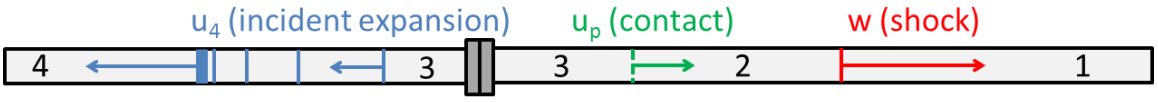

After expansion fan reflection:

Given: $\frac{p_4}{p_1}, \gamma_1, \gamma_4, T_1, T_4$

Solving for: w (shock wave speed), u_p (contact surface speed), u_4 (incident expansion fan speed), u_5 (reflected expansion fan speed)

First the initial speeds of sound, a_1 and a_4, were determined by:

$$a = \gamma RT \qquad \text{A1}$$

Where R is the specific gas constant for air ($287.06 \frac{J}{kgK}$). The pressure ratio across the shock wave (p_2/p_1) was then calculated iteratively through the following:

$$\frac{p_4}{p_1} = \frac{p_2}{p_1}\left\{1 - \frac{(\gamma_4 - 1)\left(\frac{a_1}{a_4}\right)\left(\frac{p_2}{p_1} - 1\right)}{2\gamma_1\left[2\gamma_1 + (\gamma_1 + 1)\left(\frac{p_2}{p_1} - 1\right)\right]}\right\}^{-\frac{2\gamma_4}{\gamma_4 - 1}} \quad \text{A2}$$

With the shock wave pressure ratio, the shock wave speed and contact surface speed were then calculated using equations A3 and A4, respectively.

$$w = a_1\sqrt{\frac{\gamma + 1}{2\gamma}\left(\frac{p_2}{p_1} - 1\right) + 1} \quad \text{A3}$$

$$u_p = \frac{a_1}{\gamma}\left(\frac{p_2}{p_1} - 1\right)\left(\frac{\frac{2\gamma}{\gamma + 1}}{\frac{p_2}{p_1} + \frac{\gamma - 1}{\gamma + 1}}\right)^{\frac{1}{2}} \quad \text{A4}$$

The expansion fan was analyzed using the method of characteristics of finite nonlinear waves. For further details, see (Anderson 2004) and the MATLAB script in Appendix B.

Appendix B: MATLAB Code

`shocktube_refvel`: given initial driver and driven conditions, calculate shock wave and contact surface properties.

```
function [ w,u_p,p2top1,a4,T2,Ms ] = shocktube_refvel( driver_pressure,...
    driven_pressure,driver_temp,driven_temp,gamma )
%shock_contact_vel calculates shock wave and contact velocities
%   shock_contact_vel calculates the velocities of resulting shock wave and
%   contact of a shock tube. This function receives driver pressure and
%   temperature, driven pressure and temperature, and ratio of specific
%   heats of the fluid as input variables. This function operates under the
%   following assumptions:
%   1) The ratio of specific heats is uniform or approximately uniform
%   across the tube.
%   2) The fluid can be considered a calorically perfect gas.

% Previously: [ w,u_p,v_inc,v_ref,x_refexp,t_refexp,p2top1,a4 ] =
% shocktube_refvel( driver_pressure,driven_pressure,
% driver_temp,driven_temp,gamma,L_driver )
p4=driver_pressure;     %initialize variables using input variables
p1=driven_pressure;
t4=driver_temp;
t1=driven_temp;

%R=1716.49;      %set universal gas constant (English)
R=287.04;        %set universal gas constant (metric)

p4top1=p4/p1;   %set driver/driven ratio
a1= (gamma*R*t1)^.5;    %determine driven speed of sound
a4= (gamma*R*t4)^.5;    %determine driver speed of sound

p2top1=fzero(@(pratio) (-p4top1+pratio*(1-((gamma-1)*(a1/a4)*(pratio-1))...
    /(2*gamma*(2*gamma+(gamma+1)*(pratio-1)))^.5)^((-2*gamma)/(gamma-1))),...
    p4top1);    %determine p2/p1

%syms pratio
%p2top1=solve((-p4top1+pratio*(1-((gamma-1)*(a1/a4)*(pratio-1))...
%    /(2*gamma*(2*gamma+(gamma+1)*(pratio-1)))^.5)...
%    ^((-2*gamma)/(gamma-1)))==0);   %determine p2/p1
%p2top1=double(p2top1);
%p2top1(imag(p2top1)~=0)=[];
%p2top1=max(p2top1);

w= a1*(((gamma+1)/(2*gamma))*(p2top1-1)+1)^.5;  %calculate shock speed
u_p= a1/gamma*(p2top1-1)*((2*gamma/(gamma+1))/...
    (p2top1+(gamma-1)/(gamma+1)))^.5;   %calculate contact speed

t2tot1=p2top1*((gamma+1)/(gamma-1)+p2top1)/(1+(gamma+1)/(gamma-1)*p2top1);
T2=t2tot1*t1;
Ms=w/a1;

end
```

`refexp`: given contact surface speed and initial driver conditions, calculate incident and reflected expansion fan speeds and generate [x,t] coordinates.

```
function [ vh_inc,vh_ref,xh,th,vt_inc,vt_ref,xt,tt,a5,u ] = ...
    refexp( u_p,inc,a4,L_driver )
%REFEXP solves the reflected expansion fan problem for the head and tail
%   REFEXP uses the method of characteristics to solve the reflected expansion
%   fan problem and returns velocity, position, and time values for the
%   head and tail expansion waves.  The formatting is as follows
%
%   [vh_inc,vh_ref,xh,th,vt_inc,vt_ref,xt,tt] = refexp(u_p,inc,a4,L_driver)
%   u_p = contact or piston speed
%   inc = increment for 0:u_p
%   a4 = inital speed of sound in driver section
%   L_driver = length of the driver section
%
%   vh_inc = incident expansion wave head vel (all velocities in m/s)
%   vh_ref = reflected expansion wave head vel
%   xh = expansion wave head x location data (all distances in m)
%   th = expansion wave head time data (all times in microseconds)
%   vt_inc = incident expansion wave tail vel
%   vt_iref = reflected expansion wave tail vel
%   xt = expansion wave tail x location data
%   tt = expansion wave tail time data
%
%   This code defines n x n matrices for most variables to be calculated at
%   each point in the reflection, where n is the number of expansion waves:
%    _               _          6|/  / /    *Note the waves should all start
%   |   1  2  3    |            |\ / /       at the same x-axis location
%   |   0  4  5    |     t    | 5 /
%   |_  0  0  6   _|          4|/ 3
%                              | 2 \
%                             1|/ \ \
%                              |\__\_\_____________ x
%   The each row represents an expansion wave and the diagonal elements
%   represent the points at which each wave meets the wall
%
%   In order to utilize the vel=0 condition at the wall, the x-location and
%   time matrices were (n+1) x n, with the first row being all zeros:
%    _               _
%   |  0 0 0 0   |
%   |  1 2 3 4   |
%   |  0 5 6 7   |
%   |  0 0 8 9   |
%   |_ 0 0 0 10 _|
%
%   Useful theory:
%   J+ = u + (2*a)/(gamma-1);   J- = u - (2*a)/(gamma-1)
%   C+ = (dx/dt)+ = u + a;      C- = (dx/dt)- = u - a;
%   J+/J- is constant along C+/C- curves, respectively

gamma=1.4;

vel=0:inc:u_p;  %define vector of expansion wave velocities
nwaves=length(vel);     %determine number of expansion waves
x=zeros(nwaves+1,nwaves);   %generate zero matrix for x-location
t=x;    %generate zero matrix for time
jp=zeros(nwaves,nwaves);    %generate zero matrix for J+
jm=jp;  %generate zero matrix for J-
u=jp;   %generate zero matrix for wave velocity
a=jp;   %generate zero matrix for speed of sound
cp=jp;  %generate zero matrix for C+
cm=jp;  %generate zero matrix for C-

for i=1:nwaves      %cycle through the waves
```

```
    for j=i:nwaves      %cycle through each point of the current wave

        if i==j     %if the current point if the first point of the wave

            if i==1     %if the current wave is the first wave
                a(i,j)=a4;  %hardcode to use the given driven SOS
            else
                a(i,j)=-(gamma-1)/2*(jm(i-1,j));    %determine SOS
            end

            jp(i,j)=2/(gamma-1)*a(i,j); %calculate J/C +/- using a
            jm(i,j)=-jp(i,j);
            cp(i,j)=a(i,j);
            cm(i,j)=-cp(i,j);

            %recall the first row is zero to utilize the origin (0,0);
            %therefore, the diagonal starting with (2,1) represents the
            %point at which each expansion wave meets the wall
            x(i+1,j)=-L_driver; %at the wall, all x-values are -L_driver from the origin
            t(i+1,j)=t(i,j)-(x(i+1,j)-x(i,j))/a(i,j);   %time is calculated
            %using basic
            %kinematics

        else        %for all other points of the wave
            if i==1     %if the current wave is the first wave
                u(i,j)=vel(j-i+1);  %pull velocity from velocity vector
                a(i,j)=(gamma-1)/2*(jp(i,j-1)-u(i,j));
                jp(i,j)=jp(i,j-1);  %pull J+ from previous point on C+
                jm(i,j)=u(i,j)-2*a(i,j)/(gamma-1);  %calculated J- based on
                                                    %pulled velocity

            else
                jp(i,j)=jp(i,j-1);  %pull J+ from previous point on C+
                jm(i,j)=jm(i-1,j);  %pull J- from previous point on C-
                %solve for u and a through known J+/- values
                %J+ = u + 2/(gamma-1) --> b = A * sol
                %J- = u - 2/(gamma-1)
                A=[1 2/(gamma-1); 1 -2/(gamma-1)];
                b=[jp(i,j); jm(i,j)];
                sol=A\b;
                u(i,j)=sol(1);
                a(i,j)=sol(2);
                clear A b sol

            end
            cp(i,j)=u(i,j)+a(i,j);  %calculate C+/- with determined u and
            cm(i,j)=u(i,j)-a(i,j);  %a values

            A=[1 -cp(i,j); 1 -cm(i,j)];
            b=[x(i+1,j-1)-cp(i,j)*t(i+1,j-1); x(i,j)-cm(i,j)*t(i,j)];
            sol=A\b;
            x(i+1,j)=sol(1);
            t(i+1,j)=sol(2);
        end
    end
end
vh_inc=-a4;     %incident head velocity (m/s)
vh_ref=u_p+a(1,end);    %refected head velocity
vt_inc=u_p-a(1,end);    %incident tail velocity
vt_ref=u_p+a(end,end);  %reflected tail velocity
xh=[0, x(2,1:end)]';    %head x-location (m)
th=[0, t(2,1:end)]'*10^6;   %head time (microseconds)
xt=x(1:end,end)';   %tail x-location
tt=t(1:end,end)'*10^6;  %tail time
a5=a(end);

end
```

Appendix C: Photographs of Experimental Set-up

Figure C1: Full shock tube

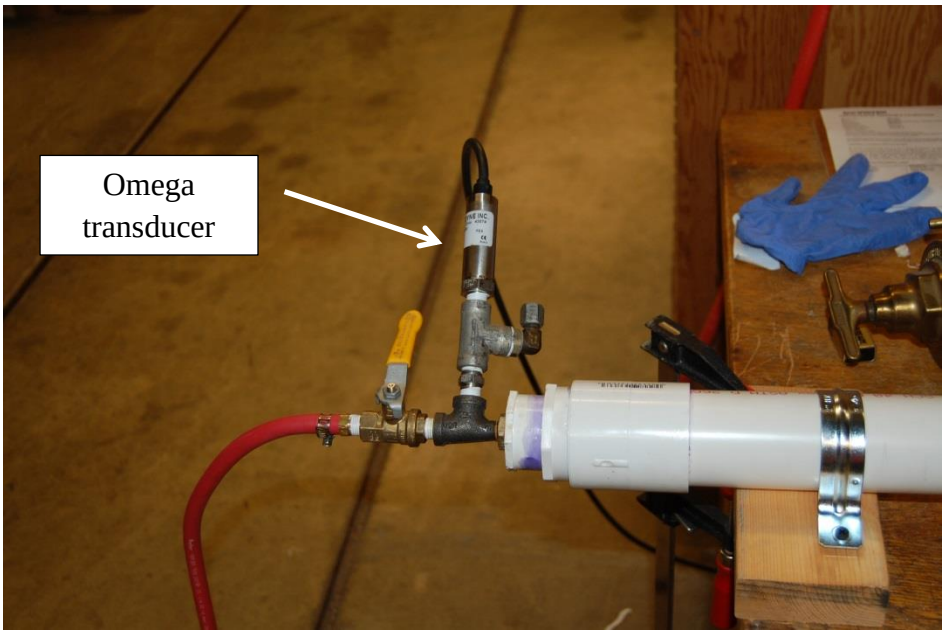

Figure C2: Omega pressure transducer for measuring driver section pressure

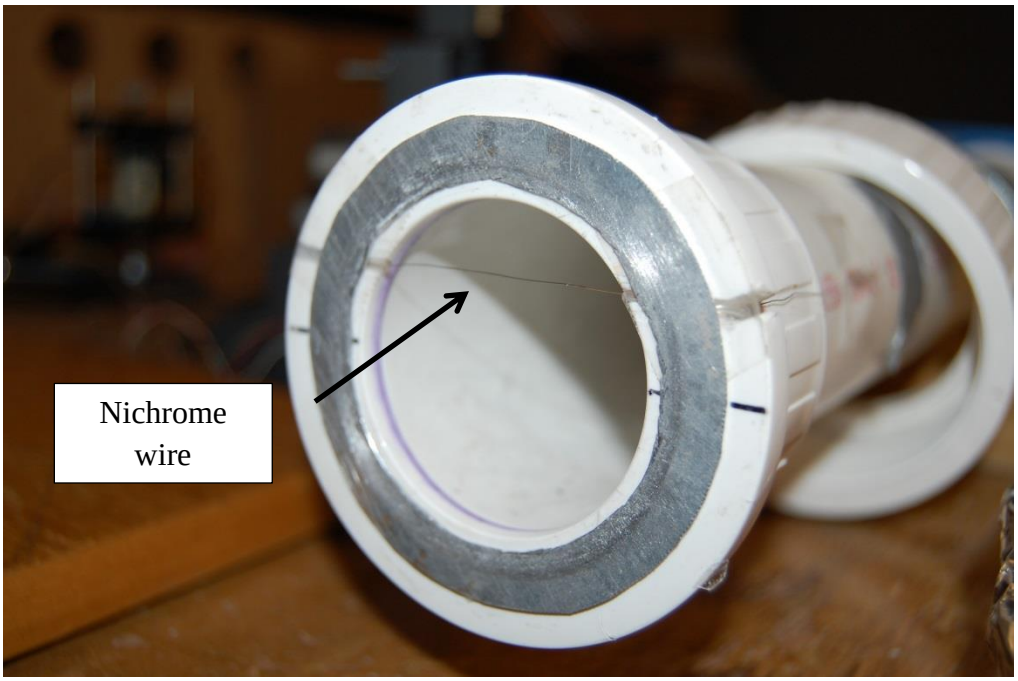

Figure C3: Diaphragm region with nichrome wire stretch across

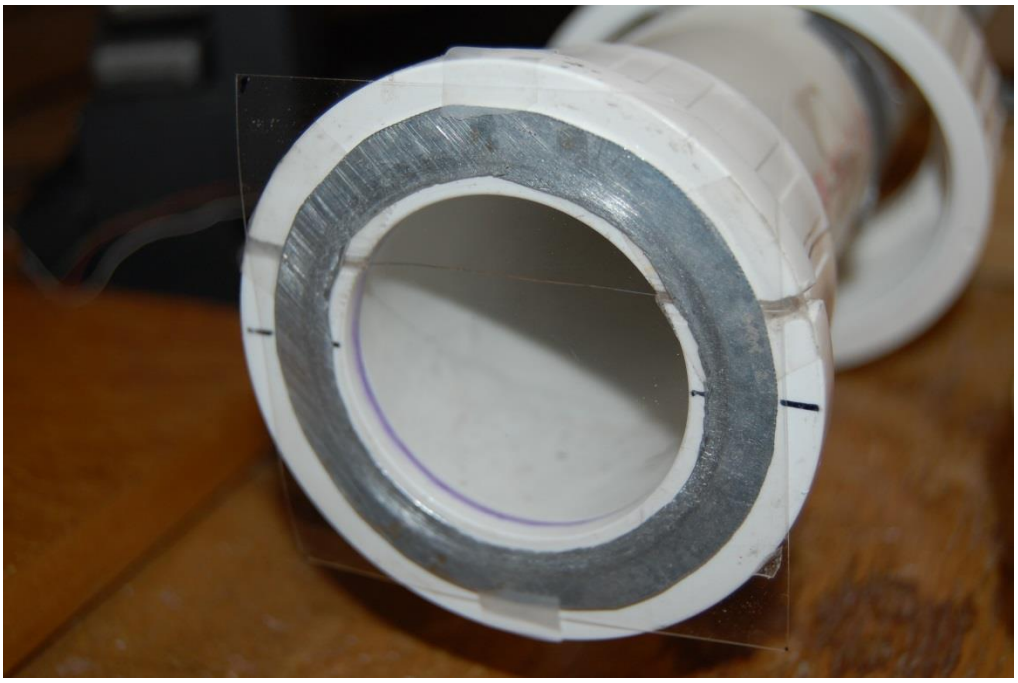

Figure C4: Acetate sheet applied to diaphragm region

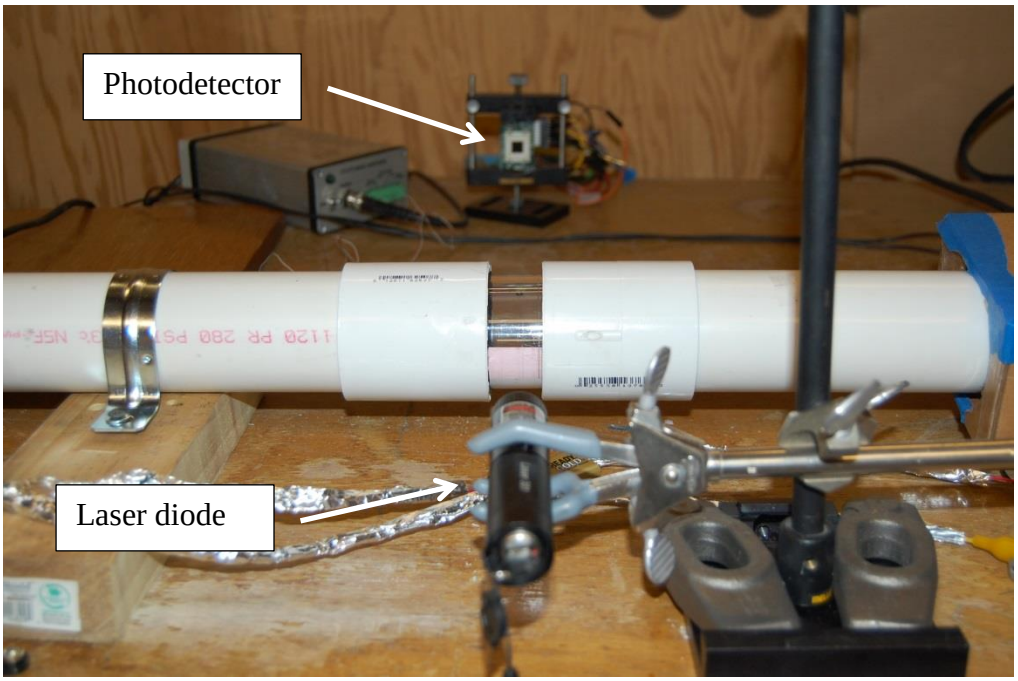

Figure C5: Laser diode and photodetector set-up

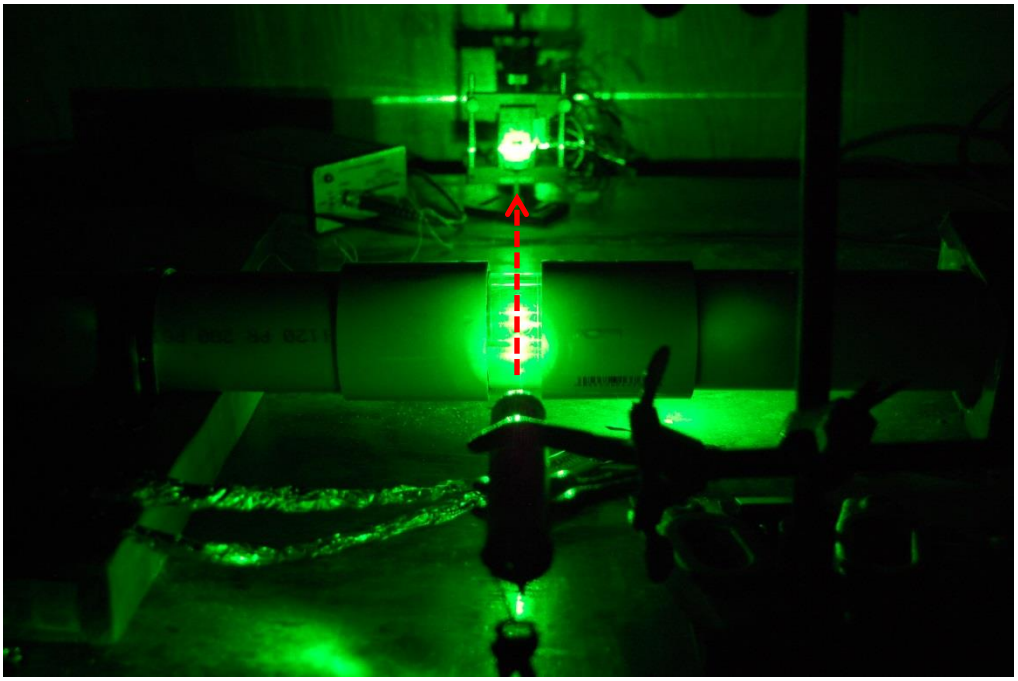

Figure C6: Laser diode and photodetector set-up, lights off

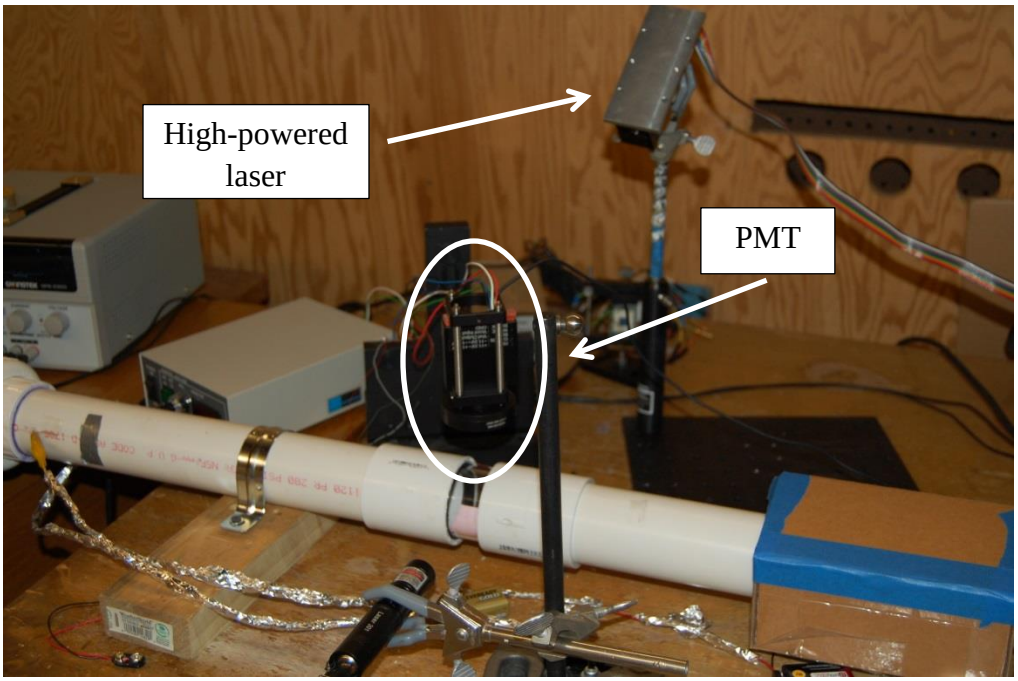

Figure C7: High-powered laser and PMT set-up

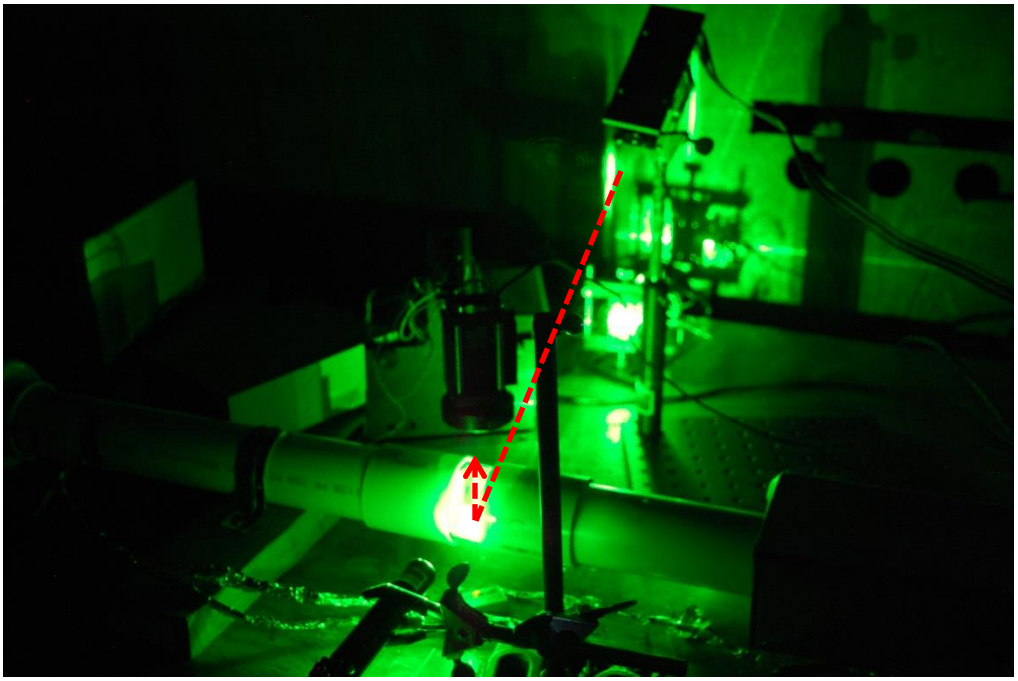

Figure C8: High-powered laser and PMT set-up, lights off